

# BRAIN-HGCN: A HYPERBOLIC GRAPH CONVOLUTIONAL NETWORK FOR BRAIN FUNCTIONAL NETWORK ANALYSIS

Junhao Jia<sup>1</sup>, Yunyou Liu<sup>1</sup>, Cheng Yang<sup>1</sup>, Yifei Sun<sup>2</sup>, Feiwei Qin<sup>1,\*</sup>, Changmiao Wang<sup>3</sup>, Yong Peng<sup>1</sup>

<sup>1</sup> Hangzhou Dianzi University, Hangzhou, China

<sup>2</sup> Zhejiang University, Hangzhou, China

<sup>3</sup> Shenzhen Research Institute of Big Data, Shenzhen, China

\* Corresponding author: qinfeiwei@hdu.edu.cn

## ABSTRACT

Functional magnetic resonance imaging (fMRI) provides a powerful non-invasive window into the brain's functional organization by generating complex functional networks, typically modeled as graphs. These brain networks exhibit a hierarchical topology that is crucial for cognitive processing. However, due to inherent spatial constraints, standard Euclidean GNNs struggle to represent these hierarchical structures without high distortion, limiting their clinical performance. To address this limitation, we propose Brain-HGCN, a geometric deep learning framework based on hyperbolic geometry, which leverages the intrinsic property of negatively curved space to model the brain's network hierarchy with high fidelity. Grounded in the Lorentz model, our model employs a novel hyperbolic graph attention layer with a signed aggregation mechanism to distinctly process excitatory and inhibitory connections, ultimately learning robust graph-level representations via a geometrically sound Fréchet mean for graph readout. Experiments on two large-scale fMRI datasets for psychiatric disorder classification demonstrate that our approach significantly outperforms a wide range of state-of-the-art Euclidean baselines. This work pioneers a new geometric deep learning paradigm for fMRI analysis, highlighting the immense potential of hyperbolic GNNs in the field of computational psychiatry.

**Index Terms**— Hyperbolic Learning, Lorentz Model, Brain Functional Networks, Computational Psychiatry

## 1. INTRODUCTION

Psychiatric and neurodevelopmental disorders impose major global burdens, yet their neural bases remain poorly understood [1, 2]. Functional magnetic resonance imaging (fMRI) has emerged as a pivotal tool in investigating these conditions due to its non-invasive nature and high-spatiotemporal resolution, which allow for the measurement of BOLD signals and facilitate the construction of brain functional networks [3, 4]. Composed of distributed brain regions and their synchronized activity, these networks exhibit a highly ordered hierarchical organization that is fundamental to the brain's ability to process and integrate information efficiently [5, 6].

However, mainstream approaches [7, 8, 9] rely on Euclidean geometric frameworks that assume a flat data space, an assumption that

This work was supported in part by the 'Pioneer' and 'Leading Goose' R&D Program of Zhejiang (No.2025C04001), Fundamental Research Funds for the Provincial Universities of Zhejiang (No. GK259909299001-006), Anhui Provincial Joint Construction Key Laboratory of Intelligent Education Equipment and Technology (No. IEET202401), and National Undergraduate Training Program for Innovation and Entrepreneurship (No.202510336076).

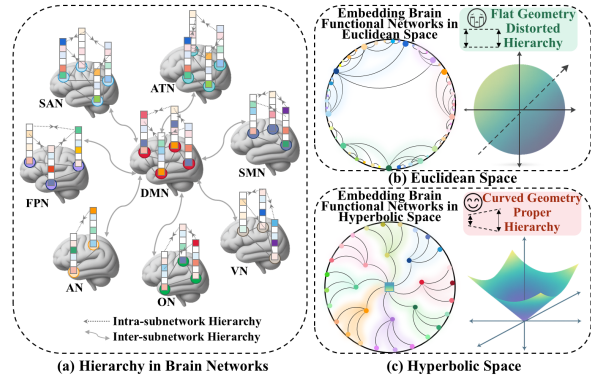


**Fig. 1:** (a) The inherent hierarchical topology of brain functional networks. (b) Euclidean embedding leads to high distortion by compressing hierarchical distances. (c) Hyperbolic embedding preserves these hierarchical relationships with high fidelity.

is misaligned with the nonlinear topological features [10] inherent to hierarchical brain networks. This makes it difficult to detect subtle hierarchical abnormalities characteristic of various neurodevelopmental disorders, ultimately impeding the development of network based biomarkers for clinical diagnosis and prognosis.

To address this methodological bottleneck, hyperbolic geometry offers a natural solution for modeling hierarchical systems due to its unique exponential expansion property [11, 12]. Unlike Euclidean space, hyperbolic space can efficiently represent hierarchical structures in lower dimensions as its metric scale expands exponentially with distance from the center [13], aligning with the core concentrated periphery divergent topology of brain networks [14]. Building on this, we propose a novel hyperbolic learning framework for brain functional network modeling that embeds functional connectivity data into hyperbolic space to leverage its exponential expansion property for the natural encoding of hierarchical relationships, as illustrated in Fig. 1. Our main contributions are:

(1) We pioneer Brain-HGCN, a geometric paradigm that embeds the brain's hierarchical topology onto the Lorentz hyperboloid to overcome Euclidean representational limitations.

(2) We architect a hyperbolic attention mechanism whose signed aggregation scheme enables geometrically principled message passing that differentiates excitatory from inhibitory pathways.

(3) We conceptualize a curvature-aware readout strategy that employs the Fréchet mean to derive distortion-free, manifold-native brain representations directly within the hyperbolic space.

## 2. PRELIMINARIES

Hyperbolic geometry offers a powerful framework for modeling hierarchical data due to its intrinsic constant negative curvature. This property allows it to embed tree-like structures with minimal distortion. To leverage this geometric property in neural networks, this section introduces the core computational tools based on the Lorentz model, which lay the foundation for the model proposed in our work.

**Lorentz Model.** The Lorentz model realizes hyperbolic space as a hyperboloid embedded in Minkowski space  $\mathbb{R}^{n+1}$ :

$$\langle \mathbf{x}, \mathbf{y} \rangle_{\mathcal{L}} = -x_0 y_0 + \sum_{i=1}^n x_i y_i, \quad (1)$$

where the first coordinate carries negative sign. The  $n$ -dimensional hyperbolic space with curvature  $-1/K < 0$  is then represented as:

$$\mathbb{H}_K^n = \{ \mathbf{x} \in \mathbb{R}^{n+1} : \langle \mathbf{x}, \mathbf{x} \rangle_{\mathcal{L}} = -K, x_0 > 0 \}, \quad (2)$$

which corresponds to the upper sheet of a two-sheeted hyperboloid. This embedding provides a smooth Riemannian manifold of constant negative curvature  $-1/K$ . The geodesic distance between two points  $\mathbf{x}, \mathbf{y} \in \mathbb{H}_K^n$  is:

$$d_K(\mathbf{x}, \mathbf{y}) = \text{arcosh} \left( -\frac{\langle \mathbf{x}, \mathbf{y} \rangle_{\mathcal{L}}}{K} \right). \quad (3)$$

This distance reflects the exponential expansion property of hyperbolic space, making it suited for encoding hierarchical relations.

**Tangent Space.** At each point  $\mathbf{x} \in \mathbb{H}_K^n$ , the tangent space is the linear space orthogonal to  $\mathbf{x}$  under the Lorentzian product:

$$T_{\mathbf{x}} \mathbb{H}_K^n = \{ \mathbf{v} \in \mathbb{R}^{n+1} : \langle \mathbf{v}, \mathbf{x} \rangle_{\mathcal{L}} = 0 \}. \quad (4)$$

The tangent space provides a local flat approximation of the curved manifold, enabling us to carry out neural operations such as linear transformations and aggregations in a consistent way.

**Exponential and Logarithmic Maps.** The exponential map projects a tangent vector back to the manifold. For  $\mathbf{v} \in T_{\mathbf{x}} \mathbb{H}_K^n$ ,

$$\exp_{\mathbf{x}}^K(\mathbf{v}) = \cosh\left(\frac{\|\mathbf{v}\|_{\mathcal{L}}}{\sqrt{K}}\right) \mathbf{x} + \sqrt{K} \sinh\left(\frac{\|\mathbf{v}\|_{\mathcal{L}}}{\sqrt{K}}\right) \frac{\mathbf{v}}{\|\mathbf{v}\|_{\mathcal{L}}}, \quad (5)$$

where  $\|\mathbf{v}\|_{\mathcal{L}} = \sqrt{\langle \mathbf{v}, \mathbf{v} \rangle_{\mathcal{L}}}$ . Intuitively,  $\exp_{\mathbf{x}}^K$  moves a geodesic distance  $\|\mathbf{v}\|_{\mathcal{L}}/\sqrt{K}$  from  $\mathbf{x}$  along the geodesic in the direction of  $\mathbf{v}$ .

The logarithmic map is the inverse, mapping a point  $\mathbf{y} \in \mathbb{H}_K^n$  back to the tangent space at  $\mathbf{x}$ :

$$\log_{\mathbf{x}}^K(\mathbf{y}) = \frac{\text{arcosh} \left( -\frac{\langle \mathbf{x}, \mathbf{y} \rangle_{\mathcal{L}}}{K} \right)}{\sqrt{\left( -\frac{\langle \mathbf{x}, \mathbf{y} \rangle_{\mathcal{L}}}{K} \right)^2 - 1}} \left( \mathbf{y} + \frac{\langle \mathbf{x}, \mathbf{y} \rangle_{\mathcal{L}}}{K} \mathbf{x} \right). \quad (6)$$

This operation returns the tangent vector at  $\mathbf{x}$  that points towards  $\mathbf{y}$ , whose Lorentzian norm satisfies  $\|\log_{\mathbf{x}}^K(\mathbf{y})\|_{\mathcal{L}} = \sqrt{K} d_K(\mathbf{x}, \mathbf{y})$ .

## 3. METHODOLOGY

As illustrated in Fig. 2, we propose the Brain-HGCN framework, which embeds fMRI data into hyperbolic space and exploits this space's intrinsic exponential expansion to naturally capture and encode the hierarchical organizational principles of the brain.

### 3.1. Subject-wise Brain Network Construction

For each subject, we build a weighted, undirected, signed graph  $\mathcal{G} = (\mathcal{V}, \mathcal{E}, \mathbf{A}^{(+)}, \mathbf{A}^{(-)})$ . The nodes  $\mathcal{V}$  represent Regions of Interest (ROIs) from the AAL-116 atlas. The initial feature for each node  $v_i$  is its corresponding ROI-averaged time series,  $\mathbf{x}_i^{0,E} \in \mathbb{R}^T$ , where  $T$  is the number of time points. Edges  $\mathcal{E}$  are weighted by the Pearson correlation  $C_{ij}$  between nodal time series. To preserve signed coupling, we construct a sparse, symmetric graph by retaining the top- $k$  positive and negative connections for each node:

$$A_{ij}^{(+)} = \max(C_{ij}, 0), \quad A_{ij}^{(-)} = \max(-C_{ij}, 0). \quad (7)$$

### 3.2. Hyperbolic Neural Network Primitives

We instantiate the model on the hyperboloid  $\mathbb{H}_K^d$  with constant negative curvature  $-1/K < 0$ . Each layer learns its own curvature  $K_{\ell} > 0$ . Let  $\mathbf{o} = (\sqrt{K_0}, 0, \dots, 0)$  denote the origin. We use the exponential/logarithmic maps  $\exp^K(\cdot)(\cdot)$  and  $\log^K(\cdot)(\cdot)$ . Supercripts  $E/H$  distinguish Euclidean and hyperbolic quantities.

**Input lifting.** Euclidean node features are lifted to the manifold via the exponential map at the origin:

$$\mathbf{x}_i^{0,H} = \exp_{\mathbf{o}}^{K_0}((0, \mathbf{x}_i^{0,E})). \quad (8)$$

**Hyperbolic linear transform and bias.** Let  $\mathbf{W}_{\ell}$  be a weight matrix acting in the origin tangent space. We define the hyperbolic matrix–vector product and bias addition by:

$$\begin{aligned} \mathbf{W}_{\ell} \otimes_{K_{\ell-1}} \mathbf{x}_i^{\ell-1,H} &= \exp_{\mathbf{o}}^{K_{\ell-1}} \left( \mathbf{W}_{\ell} \log_{\mathbf{o}}^{K_{\ell-1}}(\mathbf{x}_i^{\ell-1,H}) \right), \\ \mathbf{x} \oplus_K \mathbf{b} &= \exp_{\mathbf{x}}^K \left( \text{PT}_{\mathbf{o} \rightarrow \mathbf{x}}^K(\mathbf{b}) \right). \end{aligned} \quad (9)$$

where  $\mathbf{b}_{\ell} \in T_{\mathbf{o}} \mathbb{H}_{K_{\ell-1}}$  is a bias in the origin tangent space and  $\text{PT}_{\mathbf{o} \rightarrow \mathbf{x}}^K$  denotes parallel transport to the center point's tangent space. The transformed representation is:

$$\mathbf{h}_i^{\ell,H} = (\mathbf{W}_{\ell} \otimes_{K_{\ell-1}} \mathbf{x}_i^{\ell-1,H}) \oplus_{K_{\ell-1}} \mathbf{b}_{\ell}. \quad (10)$$

### 3.3. Hyperbolic Attention with Signed Aggregation

We introduce a hyperbolic attention layer designed for the signed topology of brain networks. Let  $\mathbf{x}_i^{\ell-1,H}$  be the feature of node  $i$  from the previous layer. First, we apply a hyperbolic linear transformation and add a bias to obtain an intermediate representation:

$$\mathbf{h}_i^{\ell,H} = (\mathbf{W}_{\ell} \otimes_{K_{\ell-1}} \mathbf{x}_i^{\ell-1,H}) \oplus_{K_{\ell-1}} \mathbf{b}_{\ell}. \quad (11)$$

**Lorentzian Attention Mechanism.** We adapt multi-head attention to the Lorentz model. For each head  $m$ , queries ( $\mathbf{q}$ ), keys ( $\mathbf{k}$ ), and values ( $\mathbf{v}$ ) are generated via linear maps and attention scores are computed using the Lorentzian inner product  $\langle \cdot, \cdot \rangle_{\mathcal{L}}$ , which naturally arises from the geometry of the Lorentz model:

$$s_{ij}^{(m)} = \frac{\langle \mathbf{q}_i^{(m)}, \mathbf{k}_j^{(m)} \rangle_{\mathcal{L}}}{\sqrt{d} \tau_{\ell}}, \quad \text{where} \quad \tau_{\ell} = \tau_0 / \sqrt{K_{\ell-1}}. \quad (12)$$

To handle signed edges, we normalize scores separately over excitatory (+) and inhibitory (-) neighborhoods:

$$\begin{aligned} w_{ij}^{(m,+)} &= \text{softmax}_{j \in \mathcal{N}_i^{(+)}}(s_{ij}^{(m)}), \\ w_{ij}^{(m,-)} &= \text{softmax}_{j \in \mathcal{N}_i^{(-)}}(s_{ij}^{(m)}). \end{aligned} \quad (13)$$

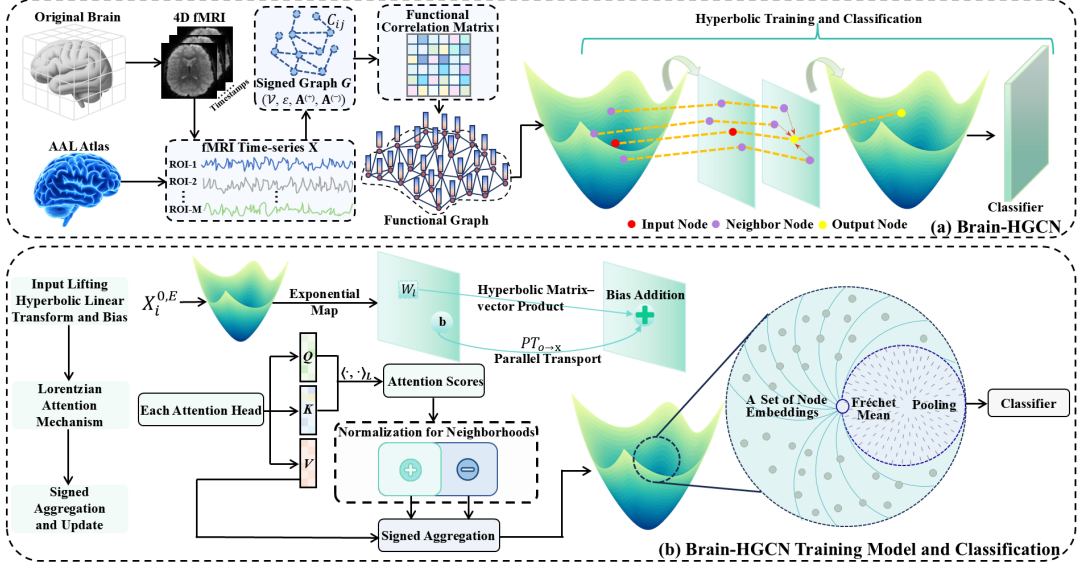


**Fig. 2:** The overview of our proposed Brain-HGCN framework. (a) Illustrates the process of constructing a signed functional graph from fMRI data for end-to-end classification. (b) The core model for Brain-HGCN training and classification, featuring a Lorentzian attention with signed aggregation for message passing, and a Fréchet mean readout for intrinsic graph pooling and classification.

**Signed Aggregation and Update.** The aggregation is performed in the tangent space of the central node  $\mathbf{h}_i^{\ell, H}$ . We pull from positive neighbors and push from negative ones:

$$\Delta_i^{(m)} = \sum_{j \in \mathcal{N}_i^{(+)}} w_{ij}^{(m, +)} \log_{\mathbf{h}_i^{\ell, H}}^{K_{\ell-1}} (\mathbf{v}_j^{(m)}) - \sum_{j \in \mathcal{N}_i^{(-)}} w_{ij}^{(m, -)} \log_{\mathbf{h}_i^{\ell, H}}^{K_{\ell-1}} (\mathbf{v}_j^{(m)}). \quad (14)$$

The outputs are averaged and projected back to the manifold:

$$\mathbf{y}_i^{\ell, H} = \exp_{\mathbf{h}_i^{\ell, H}}^{K_{\ell-1}} \left( \frac{1}{H} \sum_{m=1}^H \Delta_i^{(m)} \right). \quad (15)$$

Finally, we apply a Euclidean non-linearity  $\sigma$  in the origin's tangent space and map the result back to the manifold under the new layer curvature  $K_\ell$  to obtain the final node representation for this layer:

$$\mathbf{x}_i^{\ell, H} = \exp_{\mathbf{o}}^{K_\ell} \left( \sigma \left( \log_{\mathbf{o}}^{K_{\ell-1}} (\mathbf{y}_i^{\ell, H}) \right) \right). \quad (16)$$

### 3.4. Intrinsic Graph Readout and Classification

The final hyperbolic layer yields node embeddings  $\{\mathbf{x}_i^{L, H}\}_{i=1}^N$ . For graph-level classification, our intrinsic readout computes the Fréchet mean and pools in its tangent space.

**Fréchet Mean as Geometric Center.** The Fréchet mean,  $\mu_G$  generalizes the Euclidean centroid to Riemannian manifolds, defined as the point minimizing the sum of squared geodesic distances to all nodes:

$$\mu_G = \arg \min_{x \in \mathbb{H}_{K_L}^d} \frac{1}{N} \sum_{i=1}^N d_{K_L}(x, \mathbf{x}_i^{L, H})^2. \quad (17)$$

On Hadamard manifolds, this mean is unique and can be found by

Karcher flow:

$$\mathbf{v}^{(t)} = \frac{1}{N} \sum_{i=1}^N \log_{\mu^{(t)}}^{K_L} (\mathbf{x}_i^{L, H}), \quad (18)$$

$$\mu^{(t+1)} = \exp_{\mu^{(t)}}^{K_L} (\eta \mathbf{v}^{(t)}).$$

**Pooling and Classification.** With  $\mu_G$  as the anchor, we map nodes to  $T_{\mu_G}$  and average:

$$\mathbf{z}_G = \frac{1}{N} \sum_{i=1}^N \log_{\mu_G}^{K_L} (\mathbf{x}_i^{L, H}). \quad (19)$$

The Euclidean vector  $\mathbf{z}_G$  is fed to a classifier and we train end-to-end with cross-entropy loss.

## 4. EXPERIMENTS

### 4.1. Experimental Setup

We evaluate Brain-HGCN on ADHD-200 [15] and ABIDE [16] datasets. Using official preprocessing and quality control, ADHD-200 yields 776 subjects with 285 ADHD and 491 controls, and ABIDE yields 871 subjects with 403 ASD and 468 controls.

Brain-HGCN comprises 3 attention layers ( $d = 64$ ) with learnable per-layer curvature  $K_\ell$  (init=1.0) and 4 attention heads. We build sparse graphs ( $k = 10$ ) and compute the Fréchet mean over 5 iterations ( $\eta = 0.1$ ). The model was trained for 100 epochs using AdamW (lr=10<sup>-3</sup>, weight decay=5 × 10<sup>-4</sup>, batch size=32).

### 4.2. Comparison with SOTA Methods

As shown in Table 1, we compare Brain-HGCN with thirteen advanced baselines across CNN, Transformer, and GNN categories.

On ADHD-200, Brain-HGCN reaches accuracy 83.6% and AUC 90.7%, gains of 1.9 and 2.0 points over MM-GTUNets at

**Table 1:** Performance Comparison on ADHD-200 and ABIDE datasets. All results are reported as mean $\pm$ std over a 10-fold cross-validation. The top three results in each column are highlighted in **first**, **second**, and **third** place colors, respectively.

Method	ADHD-200 (ADHD)[15]				ABIDE (ASD)[16]			
	ACC (%)	SEN (%)	SPE (%)	AUC (%)	ACC (%)	SEN (%)	SPE (%)	AUC (%)
<b>CNN-based Method</b>								
VGG16 (ICLR'15)[17]	64.6 $\pm$ 3.8	59.7 $\pm$ 5.3	70.3 $\pm$ 3.1	65.0 $\pm$ 3.1	71.3 $\pm$ 3.2	73.0 $\pm$ 4.2	69.1 $\pm$ 3.9	71.0 $\pm$ 2.9
ResNet-50 (CVPR'16)[18]	68.5 $\pm$ 3.4	57.7 $\pm$ 4.8	78.1 $\pm$ 3.6	67.9 $\pm$ 3.0	72.2 $\pm$ 2.9	68.0 $\pm$ 3.3	75.6 $\pm$ 2.6	71.8 $\pm$ 2.1
BrainNetCNN (Neuro'17)[7]	68.0 $\pm$ 3.3	65.8 $\pm$ 8.3	70.4 $\pm$ 5.3	68.1 $\pm$ 4.9	67.3 $\pm$ 2.6	63.3 $\pm$ 9.4	70.5 $\pm$ 8.7	66.9 $\pm$ 6.4
MMAFN (DLCV'25)[19]	77.6 $\pm$ 2.1	75.2 $\pm$ 2.7	73.5 $\pm$ 2.1	77.4 $\pm$ 2.3	80.4 $\pm$ 1.6	79.2 $\pm$ 2.4	77.5 $\pm$ 2.1	80.1 $\pm$ 1.4
<b>Transformer-based Method</b>								
BNT (NeurIPS'22)[8]	72.8 $\pm$ 2.9	70.9 $\pm$ 4.3	73.9 $\pm$ 3.6	72.4 $\pm$ 2.8	75.9 $\pm$ 1.6	72.9 $\pm$ 5.3	69.8 $\pm$ 6.6	71.3 $\pm$ 4.2
MCPATS (JBHI'24)[20]	74.0 $\pm$ 3.3	64.3 $\pm$ 4.7	80.4 $\pm$ 2.9	72.3 $\pm$ 3.8	76.0 $\pm$ 2.6	73.2 $\pm$ 3.6	78.7 $\pm$ 2.9	76.0 $\pm$ 2.3
GBT (MICCAI'24)[21]	70.4 $\pm$ 3.6	68.1 $\pm$ 4.3	71.5 $\pm$ 3.9	69.8 $\pm$ 2.9	78.0 $\pm$ 6.6	79.5 $\pm$ 9.5	77.3 $\pm$ 4.0	78.4 $\pm$ 5.2
RTGMFF (arXiv'25)[22]	80.7 $\pm$ 2.5	79.5 $\pm$ 3.0	81.3 $\pm$ 2.8	80.4 $\pm$ 2.1	86.4 $\pm$ 1.9	84.5 $\pm$ 2.7	87.5 $\pm$ 2.3	86.0 $\pm$ 1.8
<b>GNN-based Method</b>								
BrainGNN (MIA'21)[9]	64.7 $\pm$ 3.8	67.9 $\pm$ 3.5	62.7 $\pm$ 4.1	65.3 $\pm$ 2.7	69.3 $\pm$ 3.9	66.8 $\pm$ 3.3	72.7 $\pm$ 3.4	69.8 $\pm$ 2.4
BrainGB (TMI'22)[23]	65.8 $\pm$ 2.6	61.3 $\pm$ 4.9	70.3 $\pm$ 3.8	65.8 $\pm$ 3.1	63.2 $\pm$ 2.0	63.8 $\pm$ 8.1	60.1 $\pm$ 6.9	62.0 $\pm$ 5.3
A-GCL (MIA'23)[24]	77.8 $\pm$ 4.4	76.4 $\pm$ 4.7	79.4 $\pm$ 5.3	77.9 $\pm$ 3.5	82.9 $\pm$ 2.1	82.4 $\pm$ 2.6	83.7 $\pm$ 1.9	83.1 $\pm$ 1.6
KMGCN (MIA'25)[25]	75.2 $\pm$ 2.6	72.8 $\pm$ 3.9	77.0 $\pm$ 2.6	74.2 $\pm$ 3.9	84.7 $\pm$ 1.3	83.6 $\pm$ 1.7	81.3 $\pm$ 1.4	82.4 $\pm$ 1.1
MM-GTUNets (TMI'25) [26]	81.7 $\pm$ 1.6	78.8 $\pm$ 2.9	81.1 $\pm$ 1.9	88.7 $\pm$ 1.5	83.1 $\pm$ 1.7	84.6 $\pm$ 2.1	82.3 $\pm$ 1.6	87.4 $\pm$ 1.5
<b>Brain-HGCN (Ours)</b>	83.6 $\pm$ 1.3	80.8 $\pm$ 2.7	85.8 $\pm$ 1.6	90.7 $\pm$ 1.2	88.3 $\pm$ 1.1	87.1 $\pm$ 1.2	89.7 $\pm$ 0.9	91.4 $\pm$ 0.7

**Table 2:** Ablation study on the ADHD-200 and ABIDE datasets. All results are reported as mean $\pm$ std over a 10-fold cross-validation. The top three results in each column are highlighted in **first**, **second**, and **third** place colors, respectively.

Method	ADHD-200 (ADHD)[15]				ABIDE (ASD)[16]			
	ACC (%)	SEN (%)	SPE (%)	AUC (%)	ACC (%)	SEN (%)	SPE (%)	AUC (%)
w/o Hyperbolic Geometry	78.5 $\pm$ 2.1	75.1 $\pm$ 3.5	80.3 $\pm$ 2.8	84.1 $\pm$ 1.9	82.1 $\pm$ 1.8	83.2 $\pm$ 2.5	80.5 $\pm$ 2.1	85.3 $\pm$ 1.5
w/o Fréchet Mean Readout	82.0 $\pm$ 1.5	78.9 $\pm$ 2.9	84.1 $\pm$ 1.9	88.5 $\pm$ 1.4	85.9 $\pm$ 1.3	87.5 $\pm$ 1.8	83.1 $\pm$ 1.2	89.8 $\pm$ 1.0
w/o Lorentzian Attention	81.3 $\pm$ 1.8	78.2 $\pm$ 3.1	83.5 $\pm$ 2.2	87.9 $\pm$ 1.6	85.2 $\pm$ 1.5	86.9 $\pm$ 2.0	82.8 $\pm$ 1.4	89.1 $\pm$ 1.2
w/o Signed Aggregation	80.2 $\pm$ 1.9	76.9 $\pm$ 3.3	82.8 $\pm$ 2.5	86.5 $\pm$ 1.8	84.5 $\pm$ 1.6	85.1 $\pm$ 2.2	83.7 $\pm$ 1.3	88.2 $\pm$ 1.3
<b>Brain-HGCN (Ours)</b>	83.6 $\pm$ 1.3	80.8 $\pm$ 2.7	85.8 $\pm$ 1.6	90.7 $\pm$ 1.2	87.3 $\pm$ 1.1	89.6 $\pm$ 1.2	84.3 $\pm$ 0.9	91.4 $\pm$ 0.7

81.7% and 88.7%, with sensitivity 80.8% and specificity 85.8% forming the best combination. On ABIDE, Brain-HGCN attains accuracy 88.3% and AUC 91.4%, where AUC surpasses MM-GTUNets 87.4% by 4.0 points and accuracy surpasses RTGMFF 86.4% by 1.9 points; sensitivity 87.1% and specificity 89.7% are the highest overall. Across datasets, Brain-HGCN leads on core metrics and shows stronger cross-site robustness and discriminative power.

#### 4.3. Ablation Study

Our ablation study (Table 2) quantifies each module’s contribution and confirms its cross-cohort robustness on the two datasets.

**Hyperbolic geometry.** Removing hyperbolic geometry for a Euclidean one causes the largest performance drop, proving its critical role in modeling hierarchical brain networks with low distortion.

**Fréchet mean readout.** Removing the intrinsic Fréchet mean and averaging at a fixed base point consistently degrades performance, indicating that tangent-space pooling at the intrinsic mean eliminates base-point bias and stabilizes graph-level representations.

**Lorentzian attention.** Switching to Euclidean dot-product or removing attention causes further declines, highlighting the value of a geometry-consistent similarity metric.

**Signed aggregation.** Removing the signed aggregation mech-

anism reduces accuracy, which confirms the importance of distinguishing between excitatory and inhibitory pathways.

Overall, conclusions are consistent across datasets, the components are complementary, and the full model achieves the best results on key metrics, driven by its geometric and structural design.

## 5. CONCLUSION

In this study, we introduce Brain-HGCN, a hyperbolic graph convolutional network for brain functional network analysis. Brain-HGCN leverages the Lorentz model with geometry-consistent operations to reduce hierarchical distortion, incorporates a Lorentzian multi-head attention with signed aggregation to distinctly model positive and negative couplings, and employs an intrinsic Fréchet-mean readout to enable unbiased graph-level pooling. Comparative experiments on ADHD-200 and ABIDE demonstrate superior performance over strong baselines, alongside stable training and cross-site robustness, indicating its suitability for large-scale computational psychiatry studies. Future work will extend Brain-HGCN to dynamic functional connectivity and multimodal integration, explore site harmonization and domain generalization, and develop curvature-aware, interpretable biomarkers to facilitate clinical translation.

## 6. REFERENCES

[1] Thomas R Insel and Bruce N Cuthbert, “Brain disorders? precisely,” *Science*, vol. 348, no. 6234, pp. 499–500, 2015.

[2] GBD 2019 Mental Disorders Collaborators et al., “Global, regional, and national burden of 12 mental disorders in 204 countries and territories, 1990–2019: a systematic analysis for the global burden of disease study 2019,” *The Lancet Psychiatry*, vol. 9, no. 2, pp. 137–150, 2022.

[3] Seiji Ogawa, Tso-Ming Lee, Alan R Kay, and David W Tank, “Brain magnetic resonance imaging with contrast dependent on blood oxygenation,” *Proceedings of the National Academy of Sciences*, vol. 87, no. 24, pp. 9868–9872, 1990.

[4] Michael D Fox and Michael Greicius, “Clinical applications of resting state functional connectivity,” *Frontiers in Systems Neuroscience*, vol. 4, pp. 1443, 2010.

[5] David Meunier, Renaud Lambiotte, Alex Fornito, Karen Ernsche, and Edward T Bullmore, “Hierarchical modularity in human brain functional networks,” *Frontiers in Neuroinformatics*, vol. 3, pp. 571, 2009.

[6] Danielle S Bassett and Michael S Gazzaniga, “Understanding complexity in the human brain,” *Trends in Cognitive Sciences*, vol. 15, no. 5, pp. 200–209, 2011.

[7] Jeremy Kawahara, Colin J Brown, Steven P Miller, Brian G Booth, Vann Chau, Ruth E Grunau, Jill G Zwicker, and Ghasan Hamarneh, “BrainNetCNN: Convolutional neural networks for brain networks; towards predicting neurodevelopment,” *NeuroImage*, vol. 146, pp. 1038–1049, 2017.

[8] Xuan Kan, Wei Dai, Hejie Cui, Zilong Zhang, Ying Guo, and Carl Yang, “Brain Network Transformer,” *Advances in Neural Information Processing Systems*, vol. 35, pp. 25586–25599, 2022.

[9] Xiaoxiao Li, Yuan Zhou, Nicha Dvornek, Muhan Zhang, Siyuan Gao, Juntang Zhuang, Dustin Scheinost, Lawrence H Staib, Pamela Ventola, and James S Duncan, “BrainGNN: Interpretable brain graph neural network for fMRI analysis,” *Medical Image Analysis*, vol. 74, pp. 102233, 2021.

[10] Maximillian Nickel and Douwe Kiela, “Poincaré embeddings for learning hierarchical representations,” *Advances in Neural Information Processing Systems*, vol. 30, 2017.

[11] Dmitri Krioukov, Fragkiskos Papadopoulos, Maksim Kitsak, Amin Vahdat, and Marián Boguná, “Hyperbolic geometry of complex networks,” *Physical Review E—Statistical, Nonlinear, and Soft Matter Physics*, vol. 82, no. 3, pp. 036106, 2010.

[12] Cole Baker, Isabel Suárez-Méndez, Grace Smith, Elisabeth B Marsh, Michael Funke, John C Mosher, Fernando Maestú, Mengjia Xu, and Dimitrios Pantazis, “Hyperbolic graph embedding of meg brain networks to study brain alterations in individuals with subjective cognitive decline,” *IEEE Journal of Biomedical and Health Informatics*, vol. 28, no. 12, pp. 7357–7368, 2024.

[13] Octavian Ganea, Gary Bécigneul, and Thomas Hofmann, “Hyperbolic neural networks,” *Advances in Neural Information Processing Systems*, vol. 31, 2018.

[14] Martijn P Van Den Heuvel and Olaf Sporns, “Rich-club organization of the human connectome,” *Journal of Neuroscience*, vol. 31, no. 44, pp. 15775–15786, 2011.

[15] Pierre Bellec, Carlton Chu, Francois Chouinard-Decorte, Yasmine Benhajali, Daniel S Margulies, and R Cameron Craddock, “The neuro bureau ADHD-200 preprocessed repository,” *NeuroImage*, vol. 144, pp. 275–286, 2017.

[16] Adriana Di Martino, Chao-Gan Yan, Qingyang Li, Erin Denio, Francisco X Castellanos, Kaat Alaerts, Jeffrey S Anderson, Michal Assaf, Susan Y Bookheimer, Mirella Dapretto, et al., “The autism brain imaging data exchange: towards a large-scale evaluation of the intrinsic brain architecture in autism,” *Molecular Psychiatry*, vol. 19, no. 6, pp. 659–667, 2014.

[17] Karen Simonyan and Andrew Zisserman, “Very deep convolutional networks for large-scale image recognition,” *International Conference on Learning Representations*, 2015.

[18] Kaiming He, Xiangyu Zhang, Shaoqing Ren, and Jian Sun, “Deep residual learning for image recognition,” in *Proceedings of the IEEE Conference on Computer Vision and Pattern Recognition*, 2016, pp. 770–778.

[19] Junhao Jia, Ruoyu Liang, Yi Ding, Chi Zhang, Yangming Li, Changmiao Wang, Feiwei Qin, Guodao Zhang, Xinjun Miao, Ahmed Elazab, et al., “MMAFN: Multi-modal attention fusion network for attention-deficit hyperactivity disorder classification,” in *2025 IEEE 2nd International Conference on Deep Learning and Computer Vision (DLCV)*. IEEE, 2025, pp. 1–5.

[20] Ning Jiang, Gongshu Wang, Chuyang Ye, Tiantian Liu, and Tianyi Yan, “Multi-task collaborative pre-training and adaptive token selection: A unified framework for brain representation learning,” *IEEE Journal of Biomedical and Health Informatics*, vol. 28, no. 9, pp. 5528–5539, 2024.

[21] Zhihao Peng, Zhibin He, Yu Jiang, Pengyu Wang, and Yixuan Yuan, “GBT: Geometric-oriented brain Transformer for autism diagnosis,” in *International Conference on Medical Image Computing and Computer-Assisted Intervention*. Springer, 2024, pp. 142–152.

[22] Junhao Jia, Yifei Sun, Yunyou Liu, Cheng Yang, Changmiao Wang, Feiwei Qin, Yong Peng, and Wenwen Min, “RTGMFF: Enhanced fmri-based brain disorder diagnosis via roi-driven text generation and multimodal feature fusion,” *arXiv preprint arXiv:2509.03214*, 2025.

[23] Hejie Cui, Wei Dai, Yanqiao Zhu, Xuan Kan, Antonio Aodong Chen Gu, Joshua Lukemire, Liang Zhan, Lifang He, Ying Guo, and Carl Yang, “BrainGB: a benchmark for brain network analysis with graph neural networks,” *IEEE Transactions on Medical Imaging*, vol. 42, no. 2, pp. 493–506, 2022.

[24] Shengjie Zhang, Xiang Chen, Xin Shen, Bohan Ren, Ziqi Yu, Haibo Yang, Xi Jiang, Dinggang Shen, Yuan Zhou, and Xiao-Yong Zhang, “A-GCL: Adversarial graph contrastive learning for fmri analysis to diagnose neurodevelopmental disorders,” *Medical Image Analysis*, vol. 90, pp. 102932, 2023.

[25] Xianhua Zeng, Jianhua Gong, Weisheng Li, and Zhuoya Yang, “Knowledge-driven multi-graph convolutional network for brain network analysis and potential biomarker discovery,” *Medical Image Analysis*, vol. 99, pp. 103368, 2025.

[26] Luhui Cai, Weiming Zeng, Hongyu Chen, Hua Zhang, Yueyang Li, Yu Feng, Hongjie Yan, Lingbin Bian, Wai Ting Siok, and Nizhuan Wang, “MM-GTUNets: Unified multi-modal graph deep learning for brain disorders prediction,” *IEEE Transactions on Medical Imaging*, 2025.